Vibrational Density of States and Elastic Properties of Cross-Linked Polymers: Combining Inelastic Light and Neutron Scattering

ARTICLE *in* THE JOURNAL OF PHYSICAL CHEMISTRY B · DECEMBER 2014

Impact Factor: 3.3 · DOI: 10.1021/jp410448y · Source: PubMed

11 AUTHORS, INCLUDING:

Gino Mariotto
University of Verona
271 PUBLICATIONS **3,238** CITATIONS
SEE PROFILE

Andrea Mele
Politecnico di Milano
208 PUBLICATIONS **2,716** CITATIONS
SEE PROFILE

Barbara Rossi
Elettra, Sincrotrone Trieste S.C.p.A.
63 PUBLICATIONS **430** CITATIONS
SEE PROFILE

Francesco Trotta
Università degli Studi di Torino
150 PUBLICATIONS **2,501** CITATIONS
SEE PROFILE

THE JOURNAL OF PHYSICAL CHEMISTRY B

Article

pubs.acs.org/JPCB

Vibrational Density of States and Elastic Properties of Cross-Linked Polymers: Combining Inelastic Light and Neutron Scattering

Vincenza Crupi,[†] Aldo Fontana,[‡] Marco Giarola,[§] Stéphane Longeville,[∥] Domenico Majolino,[†] Gino Mariotto,[§] Andrea Mele,[⊥] Alessandro Paciaroni,[#] Barbara Rossi,*[,‡] Francesco Trotta,[▽] and Valentina Venuti[†]

[†]Department of Physics and Earth Sciences, University of Messina, CNISM UdR Messina, Viale Ferdinando Stagno D'Alcontres 31, 98166 Messina, Italy

[‡]Department of Physics, University of Trento, Via Sommarive 14, 38123 Povo, Trento, Italy

[§]Department of Computer Science, University of Verona, Strada le Grazie 15, 37134 Verona, Italy

[∥]Laboratoire Léon Brillouin (CEA/CNRS), CEA Saclay, 91191 Gif-sur-Yvette Cedex, France

[⊥]Department of Chemistry, Materials and Chemical Engineering "G. Natta", Politecnico di Milano, Piazza L. da Vinci 32, 20133 Milano, Italy

[#]Department of Physics, University of Perugia, Via A. Pascoli, 06123 Perugia, Italy

[▽]Dipartimento di Chimica, Università di Torino, Via Pietro Giuria 7, 10125 Torino, Italy

ABSTRACT: The vibrational dynamics of a new class of cross-linked polymers made up of cyclodextrins is here investigated in the microscopic range by the joint use of light and inelastic neutron scattering experiments. The effect of increasing the connectivity of the polymeric network on the vibrational dynamics of the system is studied by exploiting the complementarity of these two different probes. The derived densities of vibrational states of the polymers evidence the presence of the characteristic anomalous excess of vibrational modes with respect to the Debye level, already observed in the low-frequency Raman spectra and referred to as boson peak (BP). The overall analysis of the spectra suggests an emerging picture in which the motions of hydrogen atoms of the polymers are progressively hampered when the cross-linking degree of the covalent network increases. At the same time, the frequency and intensity of the BP are found to significantly change by increasing the cross-linking degree of the polymeric network, as clearly suggested by the existence of a scaling-law for the BP evolution. These findings support the conclusion that the growing of the covalent connectivity of the system induces a general modifications of the elastic properties of these cyclodextrin-based polymers, which are, once again, modulated by the cross-linking agent/cyclodextrin molar ratio.

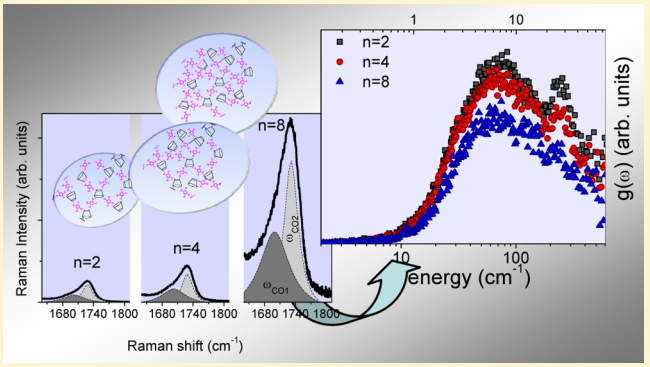

INTRODUCTION

In the past few years, a great effort has been devoted to the study of glass-forming systems due to the fact that many commonly used materials have a disordered nature. As a matter of fact, a large variety of polymers and molecular systems exhibit full or partial amorphous state.[1]

In particular, cross-linked polymers find many important uses in technology and are considered a very versatile class of materials with tailored properties at different length scales.[2] Recently, novel key applications of cross-linked polymers were proposed in the fast-growing field of drug delivery, tissue engineering, and regenerative medicine.[3−5] In the specific case of noncrystalline polymers, a thorough and systematic characterization at molecular level of their structure and dynamics is a key and preliminary step in view of the design of the functional properties.

Cyclodextrins (CDs) are natural, cyclic oligomers of amylose with well-known and well-consolidated applications as biocompatible drug carriers.[6−8] CDs are characterized by the presence of a macro-ring originated by *D*-glucopyranose units linked together via $\alpha(1\rightarrow4)$ glycoside linkages. The most common CDs are made of six, seven, or eight glucopyranose units and are generally referred to as α-, β-, and γ-CD in the order.

The several OH groups on each CD units (e.g., 21 OH groups per molecule in β-CD) are available as reactive groups for polycondensation reactions with suitable reactants − for example, activated tetracarboxylic acids derivatives − leading to

Received: October 22, 2013
Revised: December 28, 2013
Published: December 30, 2013

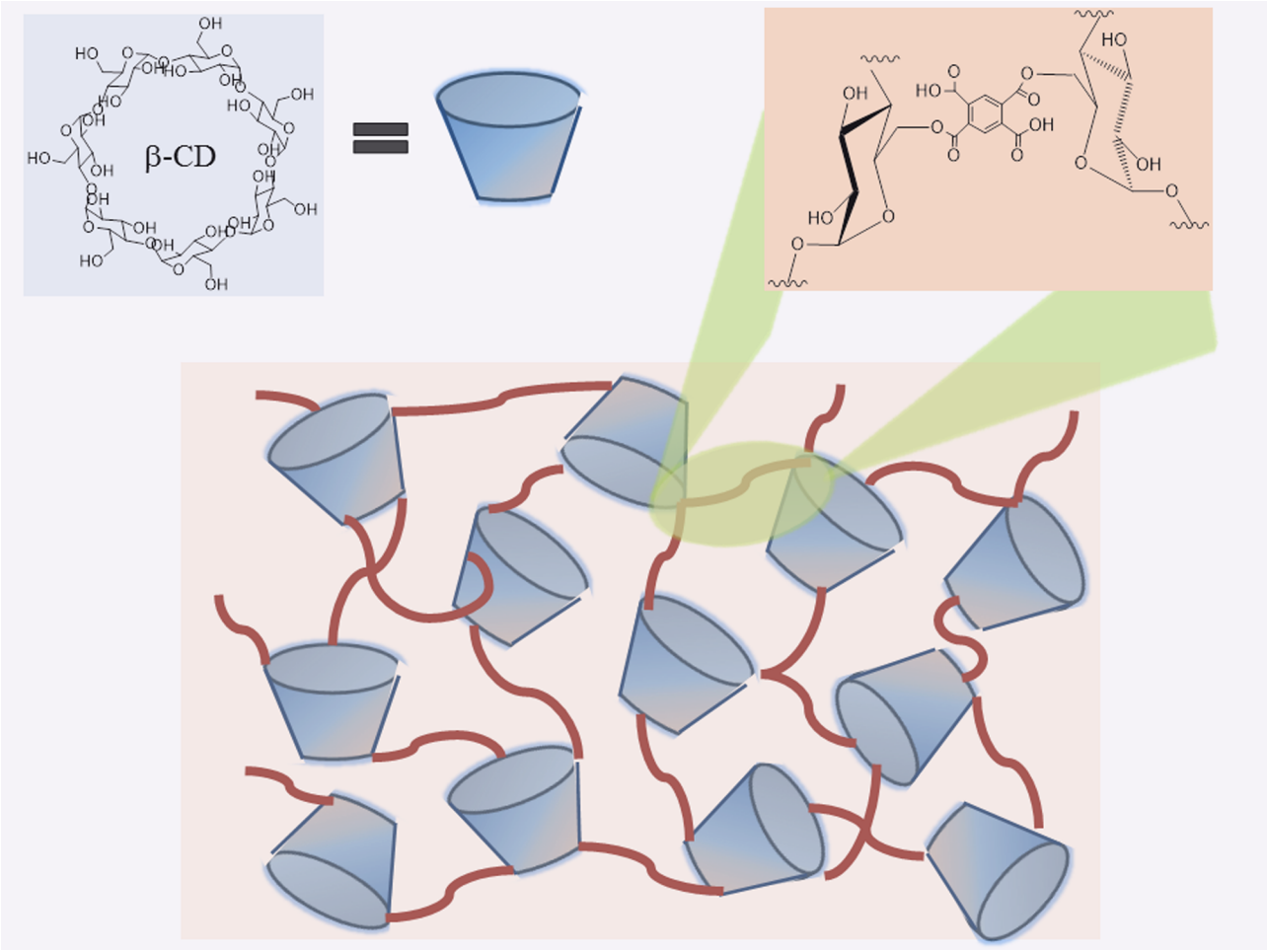

Figure 1. Schematic representation of the formation of nanosponges polymeric network from the reaction between β-CD and PMA.

cross-liked, nanoporous polymers. Such polymeric systems are referred to as cyclodextrin nanosponges (CDNSs).[8−13] CDNSs are characterized by the presence of both hydrophilic and hydrophobic cavities in the polymeric network and by the possibility of modulating the swelling capability by a careful choice of the polymerization conditions.[13]

Some types of CDNS showed interesting properties of absorption, adsorption, and release of many biologically active molecules, such as acyclovir,[14] camptothecin,[15] or paclitaxel,[16] with significant applicable perspectives in emerging technologies, like nanomedicine. Additionally, and in a more general scenario, new soft materials based on CDNS found application in agriculture,[17] environmental control,[18] cosmetic, and pharmaceutical formulations.[14,19,20] Finally, the chirality of the CDNS components was recently exploited as chiral reaction environment for photochemical asymmetric synthesis, showing a surprising capability of asymmetric induction.[21,22]

The structural and dynamic characterization of CDNS is still a challenging task in soft-matter physics because thorough knowledge of these innovative materials at the molecular level is still an ambitious objective to be reached. Indeed, different factors hamper the systematic investigation of nanosponges: (i) the random nature of the growing process of the polymer, (ii) the presence of a large number of reaction sites on each CD unit, (iii) the extensive reticulation giving rise to insoluble polymers in the majority of solvents, and (iv) the intrinsic amorphous nature of the CDNS.

Despite these limitations, many efforts have been devoted to explore the structural and dynamic properties of CDNS[23−31] at the molecular level by a broad repertoire of experimental and computational techniques. In particular, in the case of ester-bridged CDNS, some previous results[23−25,27] indicate that the relative amount of cross-linking agent with respect to monomeric CD used during the synthesis of the polymer (i.e., n = cross-linking agent/CD molar ratio) significantly affects the network of the covalent bonds and noncovalent interactions − typically hydrogen bonds − connecting the CD units within the polymer.

A detailed analysis of the high-frequency vibrational dynamics of CDNS by Raman and infrared spectroscopy[25,26,28] pointed out a clear dependence of the hydrogen-bonded network involving the OH groups of the polymer on both temperature and the parameter n. More recently, the behavior of water confined in the nanopores of swollen nanosponges was also examined.[21−23,29,30] The experimental results[29,30] suggested that in the hydrogels prepared by swelling several types of CDNS with aqueous solutions both physical and covalent bonds determine the macroscopic properties of the gel phase in a complex interplay and that the parameter n played a fundamental role in defining the nano- and microscopic properties of the system.

In this work, the combined use of two different and complementary probes (light and neutrons) is exploited to obtain information about the vibrational density of states

dx.doi.org/10.1021/jp410448y | J. Phys. Chem. B 2014, 118, 624−633

(VDOS) of CDNS synthesized by polymerization of β-CD with pyromellitic anhydride (PMA)[23−25,29−31] (see Figure 1). In particular, the low-frequency regime of the inelastic light and neutron spectra of CDNS, between 0 and 150 cm^{-1} (≈ 0−18 meV) where the collective motions of the system are typically observed, is thoroughly examined. Recent works[32,33] showed how the study of the vibrational dynamics of complex molecular systems, including CD-based materials,[33] is a powerful tool for their structural characterization. Moreover, for the investigation of the dynamical contributions arising from the picosecond motions of the system (with corresponding energies between about 1−10 meV), inelastic neutron scattering (INS) is probably the most powerful experimental technique due to its typically accessible energy and momentum transfer.

Finally, the Raman and INS spectra of CDNS are presented and compared in this work to correlate the different physical quantities probed by the two complementary scattering techniques. As main result, the central role played by the molar ratio n to determine the elastic properties of nanosponges polymer network over the mesoscopic length scale is confirmed, thus adding a further contribution to the rational comprehensive view of the physical−chemical parameters driving the formation of the CDNS network.

MATERIALS AND METHODS

A. Synthesis and Purification of Nanosponges. The ester-bridged CDNSs based on PMA were obtained by following, with minor modification, the synthetic procedure already described in the Italian patent.[34]

To obtain the β-CDPMA1n polymers, the reactions of polymerization between β-CD and the cross-linking agent pyromellitic dianhydride (PMA) at PMA/β-CD molar ratios n (with n = 2, 4, 8) were conducted by dissolving the reagents in dimethyl sulfoxide (DMSO) in the presence of triethylamine and allowing them to react at room temperature for 3 h. Once the reaction was over, the solid obtained was broken up with a spatula and washed with acetone in a Soxhlet apparatus for 24 h. The pale-yellow solid material was finally dried under vacuum.

B. Raman Scattering Measurements. All Raman measurements were carried out on dried samples of CDNSs deposited on a glass slide in air and at room temperature. All spectra were obtained in backscattering geometry, in crossed polarization, and by using two different experimental setups to better explore different spectral ranges.

The spectra in the wavenumber range between 1600 and 3700 cm^{-1} were collected by using an exciting radiation at 632.8 nm (He−Ne laser, power at the output ≈ 20 mW). The laser was focused onto the sample surface with a spot size of ∼0.8 μm^2 through the 100× objective (NA = 0.9) of a microprobe setup (Horiba-Jobin-Yvon, LabRam Aramis) consisting of a 46 cm focal length spectrograph using a 1800 grooves/mm grating and a charge-coupled device (CCD) detector. The elastically scattered radiation was filtered by using a narrow-band edge filter. The resolution was ∼0.35 cm^{-1}/pixel.

The relative amplitude of the luminescence background observed in the Raman spectra in the 1600−3700 cm^{-1} spectral range was less than a few percent in all samples examined. Therefore, the experimental profiles were corrected for the luminescence background by subtracting an interpolating baseline modeled as a linear function.

Two Lorentzian functions centered at about 1700 and 1730 cm^{-1} were used to fit the Raman spectra in the C═O stretching region. A fitted range of ∼200 cm^{-1} (1600−1800 cm^{-1}) was considered. For each fitting session, multiple iterations were performed until converging solution was reached by minimizing, in the meanwhile, the value of chi-square.

Low-wavenumber Raman spectra of CDNSs were recorded over the wavenumber range between 1.3 and 400 cm^{-1} by using a triple-monochromator spectrometer (Horiba-Jobin Yvon, model T64000) set in double-subtractive/single configuration and equipped with holographic grating 1800 grooves/mm. Micro-Raman spectra were excited by the 647.1 nm wavelength of an argon/krypton ion laser and detected by a CCD detector cryogenically cooled by liquid nitrogen. Exciting radiation was focused onto the sample surface with a spot size of ∼1 μm^2 through a 80× objective with NA = 0.75. The resolution was ∼0.36 cm^{-1}/pixel.

C. Neutron Scattering Experiments. Neutron scattering experiments were performed at Laboratoire Léon Brillouin (LLB, Saclay, France) using the time-of-flight (TOF) spectrometer MIBEMOL.

Measurements were carried out at 150 and 300 K using neutrons with an incident wavelength of 6 Å, with a Q-independent experimental elastic energy resolution of 92.7 μeV (0.7 cm^{-1}) (defined as the full width at half-maximum of a vanadium standard). The covered Q range was from 0.49 to 1.73 $Å^{-1}$. The recorded spectra were binned into 10 groups to improve the counting statistics. The explored energy range was from −45 to ∼1.4 meV (about −363 ÷ 11 cm^{-1}). In all of the Figures here reported the sign of the energy transfer was reversed for sake of simplicity.

A standard indium sealed, flat aluminum cell with a thickness of 0.2 mm internal spacing was used as sample holder. For each measurement, the sample holder was placed at an angle of 135° with respect to the incident beam direction. The time of data acquisition was about 8 h. About 96% transmission was obtained for all investigated samples.

The measured TOF spectra were analyzed with QENSH data treatment program, available at LLB. The software allows, inter alia, the correction of the detector efficiency by normalization to vanadium spectra, the correction for the empty cell, the transformation of the TOF spectra into energy spectra, and the data grouping to improve the corresponding signal/noise ratio.

D. Theoretical Background. It is well known[35−37] that Raman scattering experiments allow us to probe the fluctuations of the polarizability tensor of a system due to its elementary excitations, like vibrations. In the specific case of disordered systems, these excitation modes are expected to show a continuous frequency distribution, extending from zero up to about the Debye frequency of the material. Under the Born−Oppenheimer approximation, the polarizability fluctuations depend linearly on the atomic displacements. Consequently, the Raman spectral density reflects the VDOS.

Generally speaking, the experimental Raman intensity $I_{Raman}(\omega,T)$ can be related to the VDOS $g(\omega)$[38] by the relation:

$$I_{Raman}(\omega, T) \propto \frac{g^R(\omega)[n(\omega, T) + 1]}{\omega} \quad (1)$$

where $g^R(\omega)$ is the convolution of the VDOS $g(\omega)$ with the light-to-excitation coupling factor $C(\omega)$:

dx.doi.org/10.1021/jp410448y | J. Phys. Chem. B 2014, 118, 624−633

$$g^R(\omega) = \int C(\omega - \omega')g(\omega')\,d\omega' \quad (2)$$

and $n(\omega,T) = [\exp(\hbar\omega/k_BT)-1]^{-1}$ is the Bose−Einstein occupation number. On the basis of Shuker−Gammon model,[35] we can write, in the low-frequency regime, that:

$$g^R(\omega) = C(\omega)g(\omega) \quad (3)$$

The Raman coupling function $C(\omega)$ is a priori unknown,[36,37] and it can be experimentally obtained by measuring $g(\omega)$ with an independent probe, for example, by means of INS measurements.[33]

The intensity measured in the neutron scattering experiments corresponds to the incoherent double-differential cross section. For the systems under investigation, the dominant contribution to the revealed signal is due to the large number of hydrogen atoms, characterized by a very large, mostly incoherent, neutron cross section. Therefore, the neutron scattered intensity can be related to the so-called incoherent dynamical structure factor (or incoherent scattering function) $S_{inc}(Q,\omega)$.[39] In the one-phonon approximation, $S_{inc}(Q,\omega)$ can be written, at a given temperature, T, as:[39]

$$S_{inc}(Q,\omega) = e^{-2W(Q,T)}\{A_0(Q)\delta(\omega) + [1 - A_0(Q)]\, S_{QE}(Q,\omega) + S_{INEL}(Q,\omega)\} \otimes R(Q,\omega) \quad (4)$$

where $A_0(Q)$ is the so-called elastic incoherent structure factor, $S_{INEL}(Q,\omega)$ represents the inelastic incoherent scattering function, and $2W(Q,T) = Q^2\langle u^2(T)\rangle$ is the Debye−Waller factor (DWF) that describes the Gaussian Q-dependence due to the vibrational atomic mean square displacement $\langle u^2(T)\rangle$.

Because of the low energy of the incident neutrons of the experiment performed in this work, the INS spectrum is mainly an energy-gain spectrum because neutrons gain energy by excited vibrational modes. Nuclear interactions are not subject to dipole or polarizability selection rules, thus making INS a complementary technique with respect to Raman scattering.

From the function $S_{INEL}(Q,\omega)$, the one-phonon VDOS can be directly estimated through the relation:[40]

$$g(\omega, Q) = \frac{2M\hbar\omega S_{INEL}(Q,\omega)}{Q^2\{1 + n(\omega,T)\}\exp\{-2W(Q,T)\}} \quad (5)$$

where M is the mass of the scattering unit.

By integrating eq 5 over the entire angular range, we can calculate the VDOS $g(\omega)$ for all measured samples.[41]

In calculating the VDOS, no correction for multiphonon processes was attempted because these contributions are expected to be small at the temperatures and Q values covered by the present experiment. Moreover, multiple scattering components were neglected considering that, because our main goal was the relative comparison among samples with very similar total cross section, the relevant features were expected to be quite similar to the curve calculated without including multiple scattering. The estimated VDOS were normalized with respect to the number of total scattering atoms.

RESULTS AND DISCUSSION

A. Cross-Linking Degree (i.e., connectivity) of Cyclodextrin Nanosponges. As schematized in Figure 1, the reaction of polymerization between β-CD and the cross-linking agent PMA involves the formation of ester groups between adjacent molecules of CD, leading to the covalent cross-linking network of CDNS. As previously mentioned, the growing process of the polymers occurs in a random way due to the presence of a large number of reaction sites on each β-CD unit (which consist of 14 secondary and 7 primary OH groups per CD residue). Therefore, the final structure of the nanosponges strongly depends on the balance between two effects, namely, the number of reactive sites of CD effectively involved in the reaction and the steric hindrance effects progressively growing as the polycondensation occurs.

In Figure 2, the experimental Raman spectrum of β-CD is compared with the Raman profile of β-CDPMA12 nanosponge

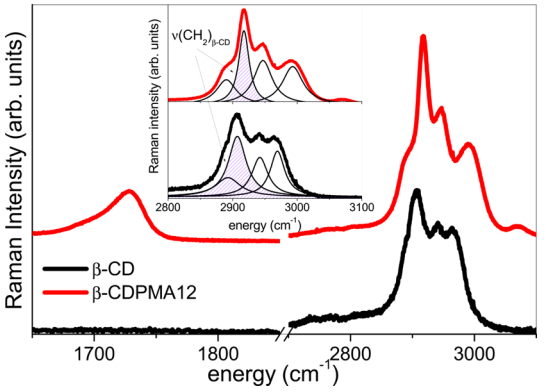

Figure 2. Comparison between the experimental Raman spectra of nanosponge β-CDPMA12 and β-CD in the wavenumber ranges 1650−1850 and 2700−3100 cm^{-1} at room temperature. Inset: spectral contributions to the mixed CH and CH_2 vibrational band with the indication of the stretching vibration $\nu(CH_2)_{\beta\text{-CD}}$ used as internal standard.

in two different spectral regions. In the wavenumber range 1650−1850 cm^{-1}, where typically the stretching vibrations of C═O groups falls, β-cyclodextrin does not show any interfering vibrational bands,[42,43] while the intense signal observed in the Raman spectrum of β-CDPMA12 nanosponge is assigned to the carbonyl stretching vibrations of esterified PMA, also in agreement with previous quantum chemical computation results.[25]

In the wavenumber range 2800−3100 cm^{-1} (Figure 2), the complex band corresponding to the vibration modes involving CH and CH_2 groups of the molecule can be clearly observed in the spectra of both β-CD and β-CDPMA12 nanosponge.

For a finer investigation, the spectral contributions in this region were properly decomposed into four components by using Lorentz functions, as shown in the inset of Figure 2. In this way, the effect of the cross-linking of cyclodextrins molecules on the spectral changes observed in the high-frequency range of CDNS spectra with respect to the profile of β-CD could be readily inspected.

As it is evident in the inset of Figure 2, a general small shift to higher energy of all spectral contributions to the CH band (with the exception of the less intense component falling at ∼2890 cm^{-1}) is observed as a consequence of assembly of cyclodextrin molecules in the polymeric network of nanosponges.

In particular, the sharp peak found at 2908 cm^{-1} in the spectrum of β-CD and assigned to the stretching vibrations of CH_2 groups of the molecule (labeled as $\nu(CH_2)_{\beta\text{-CD}}$) moves to 2917 cm^{-1} in the vibrational spectrum of β-CDPMA12. The same shift is observed for this mode in all spectra of the sample

dx.doi.org/10.1021/jp410448y | J. Phys. Chem. B 2014, 118, 624−633

of β-CDPMA1n investigated. Therefore, the band falling at 2917 cm^{-1} in the Raman spectra of nanosponges can be reasonably chosen as a reliable internal standard associated with the number of cyclodextrin units present in the CDNS polymer, as described later.

In Figure 3, the experimental Raman spectra of nanosponges β-CDPMA1n (with n = 2, 4, and 8) are shown in the wavenumber range 1640−1810 cm^{-1}, where the signals corresponding to the carbonyl stretching vibrations of esterified PMA[25] can be observed.

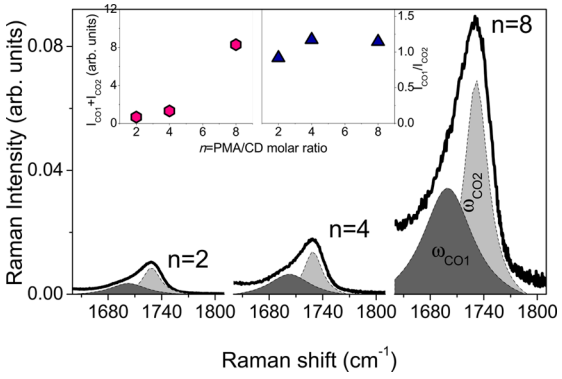

Figure 3. Experimental Raman spectra for β-CDPMA1n (with n = 2, 4, and 8 as indicated in the subpanels) in the 1640−1810 cm^{-1} wavenumber range at room temperature. Inset: total intensity I_{CO1} + I_{CO2} and ratio I_{CO1}/I_{CO2} between the intensity of the two spectral contributions to the C═O stretching band observed in Raman spectra.

The experimental profiles of Figure 3 can be deconvoluted into two separate spectral components, centered at ω_{CO1} and ω_{CO2}, by using a proper fitting procedure of the data. (See the Materials and Methods.) These components correctly describe the existing types of carbonyl stretching modes assigned, respectively, to the vibrations of the C═O belonging to the ester groups (ω_{CO1}) and to the carboxylic groups (ω_{CO2}) of the PMA-bridging residue. This assignment is derived by quantum chemical computations recently performed on a model of the bridging molecule connecting different units of CD in PMA-nanosponges.[25]

After a suitable normalization of the Raman spectra of Figure 3 to the intensity of the band falling at ∼2917 cm^{-1}, the intensity of the C═O stretching bands can be confidently associated with the population of the corresponding species. The mode at 2917 cm^{-1} assigned to the stretching vibrations of CH_2 groups of the CD units, which are not involved in the reaction of polymerization with PMA, can be used as a reliable internal standard.

The normalized total intensity I_{CO1} + I_{CO2} is reported as a function of the molar ratio n in the inset of Figure 3 (left panel). This quantity can be used as a descriptor of the cross-linking degree of the nanosponges polymeric network. A marked growing of the connectivity of the covalent cross-links among the CD units is observed for high values of n, as shown by the total intensity of the spectra reported in Figure 3.

The increase in the relative amount of PMA with respect to CD during the synthesis of the polymer does not seem to significantly affect the ratio I_{CO1}/I_{CO2} between the intensity of the two spectral contributions to the C═O stretching band observed in Raman spectra (see the other inset of Figure 3 - right panel). This finding seems to suggest that no excess of ester bonds with respect to the free carboxylic groups (or vice versa) is observed in the polymer network within the explored n range. Indeed, the connection of two CD units by one PMA results in the formation of two ester groups and two carboxylate groups. Multiple condensation, up to a maximum of four ester groups per PMA molecule, is unlikely to occur for steric and entropic reasons. On the contrary, if only one carboxylic group is converted to ester, the reaction product is a dangling pyromellitate unit attached to a single cyclodextrin units and it does not contribute to the growth of the 3D network. In the latter case, one ester function and three carboxylates are formed per each PMA unit. The experimental findings reported above − I_{CO1}/I_{CO2} virtually constant within the explored n range − indicate that the condensation of two CD units by a single PMA linker is the dominant process.

B. Vibrational Density of States of Nanosponges. In Figure 4, we report the imaginary part of the dynamical susceptibility $\chi''(\omega)$ for β-CDPMA1n (with n = 2, 4, and 8) as obtained by INS spectra, according to the relation $\chi''(\omega) = ((S_{INEL}(\omega))/[n(\omega,T) + 1])$, where $S_{INEL}(\omega)$ was calculated by integrating, for each measured sample, the Q-dependent function $S_{INEL}(Q,\omega)$ over the entire angular range. The representation of the neutron scattering intensity in terms of susceptibility is used to enhance the inelastic features of the examined samples of nanosponges at energies higher than 10 cm^{-1}. The comparison between the spectra of nanosponges in Figure 4 points out a remarkable change of the inelastic profile as a function of n. Quite interestingly, the intensity of the vibrational modes definitely decreases over the whole observed energy range as the cross-linking agent content is increased, thus suggesting that the formation of the network of the covalent and hydrogen bonds connecting the CD units has the effect of significantly hindering the vibrational modes of nanosponges in this spectral range.

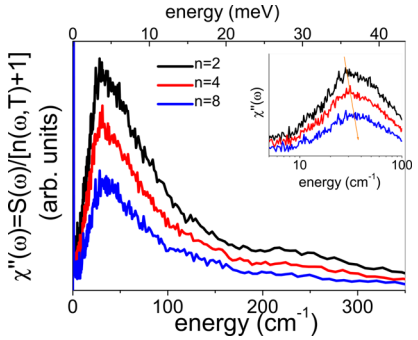

Figure 4. Dynamic susceptibility $\chi''(\omega)$ as obtained by INS spectra of β-CDEDTA1n nanosponges (n = 2, 4, 8) in the energy range 0−350 cm^{-1}. Inset: log−lin plot of the $\chi''(\omega)$ between 5 and 100 cm^{-1}.

A maximum value, found at 28−33 cm^{-1}, is observed in the susceptibility spectra of all samples of β-CDPMA1n nanosponges examined (see inset of Figure 4). This is likely to correspond to a collective mode of the hydrogen bond network, similar to those already seen in other disordered systems such as glasses[44] and proteins[45] and related to the so-called boson peak (BP) (see later). Interestingly, the maximum of $\chi''(\omega)$ tends to move to higher energy when n increases (see inset of Figure 4), in agreement with the behavior of the BP widely discussed in the following section.

Figure 5 reports the VDOS $g(\omega)$ derived for nanosponges β-CDPMA1n (n = 2, 4, 8) in the energy range 0−600 cm^{-1} and

dx.doi.org/10.1021/jp410448y | J. Phys. Chem. B 2014, 118, 624−633

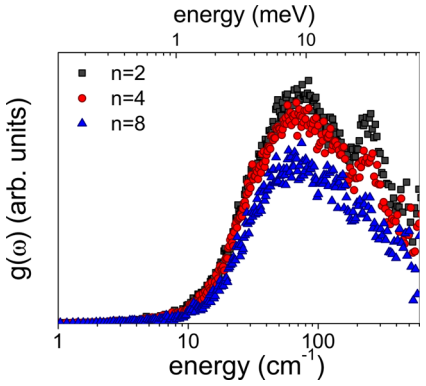

Figure 5. Log−lin plot of the experimental vibrational density of states $g(\omega)$ of β-CDPMA1n nanosponges (n = 2, 4, 8) in the energy range 0−600 cm^{-1}.

in a logarithmic−linear plot. As the VDOS were normalized with respect to the total number of scattering centers, they represent, in the incoherent approximation, the average vibrational behavior of the hydrogen atoms belonging to the system under investigation.

Figure 5 shows that increasing n, that is, of the cross-linking degree of the nanosponges network, results in the attenuation of the intensity of the vibrational modes of the polymer in the explored energy range. This finding suggests a progressive hindering of the motions of the hydrogen atoms of nanosponges, which tend to exhibit vibrational motions of smaller amplitude when included in a more interconnected pattern of covalent cross-links.

The maximum observed in the VDOS of nanosponges at ∼70 cm^{-1} (Figure 5) is nothing but the same collective excitation already previously mentioned in the discussion of the susceptibility spectra (Figure 4), only apparently shifted to higher energies due to different representation in term of the VDOS; that is, it includes the multiplying $\hbar\omega$ factor.

More interestingly, we can also clearly see in the $g(\omega)$ a peak centered at ∼240 cm^{-1}, which is a reminiscence of the vibrational feature already observed in the INS spectra of the β-cyclodextrin alone.[46] This similarity suggests that the peak found in the VDOS of nanosponges is due to optic-like modes of the β-cyclodextrin hydrogen-bond network, thus also explaining the gradual decrease in its intensity while increasing the relative weight of the cross-linker component with respect to the monomeric unit β-CD.

C. Behavior of the Boson Peak: Frequency and Intensity Variations. To better emphasize the vibrational behavior of the system in the low-frequency region up to 50 cm^{-1}, the reduced representation of the VDOS, that is, the quantity $g(\omega)/\omega^2$, is plotted in Figure 6a in comparison with the reduced Raman intensity $I^{red}(\omega)$ (Figure 6b). As expected, the VDOS of all investigated nanosponges shows an excess of vibrational states with respect to the Debye-like continuous elastic model, thus confirming the glass-like behavior of nanosponges polymers.[23,24,27] Such an excess, typically observed in inelastic light and neutron scattering spectra of disordered solids is well known as BP,[47] and it appears evident in both the panels of Figure 6.

The experimental Raman intensity was converted into the reduced Raman intensity according to the relation:

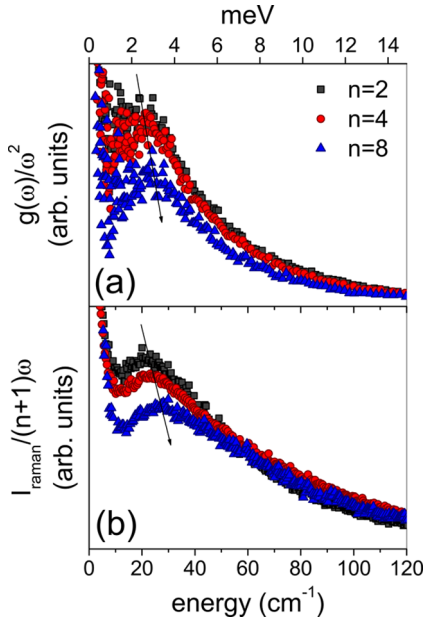

Figure 6. Reduced representation of VDOS $g(\omega)/\omega^2$ as obtained by neutron data (a) and reduced Raman intensity (b) of nanosponges β-CDPMA1n (with n = 2, 4, and 8) in the energy range 0−120 cm^{-1}. The arrows indicate the evolution of BP as a function of n.

$$I^{red}(\omega) = \frac{I_{Raman}(\omega, T)}{[n(\omega, T) + 1]\omega} = C(\omega)\frac{g(\omega)}{\omega^2} \quad (6)$$

to rule out the temperature dependence of the Raman spectra. Moreover, the quantity $I^{red}(\omega)$ indirectly provided the reduced VDOS modulated by the light-vibration coupling function $C(\omega)$.

The curves reported in Figure 6a,b display a neat maximum, referred to as BP, centered between about 18−24 and 22−27 cm^{-1} in the case of INS and Raman data, respectively.

Besides the BP, the low-frequency region (ω < 10 cm^{-1}) of the Raman spectra (Figure 6b) is characterized by the occurrence of a quasi-elastic scattering (QES) component, which appears as a broadening of the elastic line. This contribution does not significantly affect the position and the intensity of the BP (vide ultra).

The detailed inspection of the profiles of Figure 6a,b points out changes of both intensity and frequency position of the BP as a function of the parameter n. In particular, the BP shifts toward higher wavenumbers, with associated decreases in intensity, by changing the parameter n from 2 to 8.

Although several attempts have been made to explain the origin of the vibrational modes of BP,[48−51] its connection with the disordered nature of the system is quite well accepted. As already demonstrated in previous papers,[52−54] the BP spectral evolution is related to the transformation of the elastic properties of the material over a mesoscopic length scale. In fact, it was shown that the position of the maximum of BP tends to move to higher energies with increased stiffness of the system, as induced by density,[52−55] pressure,[56,57] temperature or increasing of covalent connectivity.[58] This experimental behavior was observed for both inorganic glasses[52−57] and organic glass-forming materials, such as polymers.[56,58]

The frequency evolution of BP can be highlighted by rescaling the frequency axis of the spectra of Figure 6 in terms of $\upsilon = \omega/\omega_{BP}$,[52−54,56] where ω_{BP} corresponds to the position of

dx.doi.org/10.1021/jp410448y | J. Phys. Chem. B 2014, 118, 624−633

the maximum of BP estimated from the reduced profiles of VDOS and Raman intensity.

Taking into account the proper normalization of the density of states $g(\omega)\ d\omega = g(\upsilon)\ d\upsilon$ resulting from the change of frequency variable and assuming that $C(\omega)$ in eq 6 is proportional to ω in the BP region (as verified in the following and found also in other systems[33,59,60]), we obtain the rescaled intensities:[52−54,58]

$$g(\upsilon)/\upsilon^2 = g(\omega)/\omega^2 \times \omega_{BP}^3 \quad (7)$$

$$I(\upsilon) = I^{Red}(\omega) \times \omega_{BP}^2 \quad (8)$$

where the BP positions are obtained by fitting a log−normal function to the Raman and INS data.

The so-squeezed spectra reproducing the Raman intensity and the reduced VDOS are shown in Figure 7a,b, respectively.

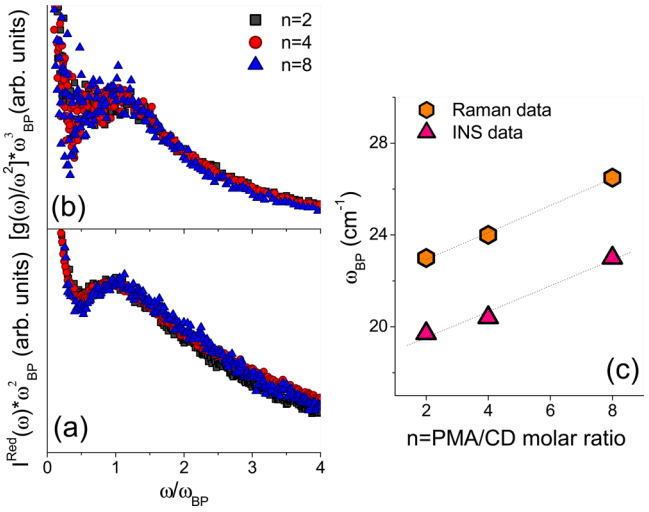

Figure 7. Master curve of the boson peak for the reduced Raman intensity (a) and $g(\omega)/\omega^2$ (b) obtained, as discussed in the text for β-CDPMA1n nanosponges (n = 2, 4, 8). (c) Frequency position estimated for ω_{BP} from Raman (orange hexagon) and INS data (pink triangles) as a function of the molar ratio n.

It is worth noting that within the experimental error the rescaled spectra corresponding to different samples of PMA-nanosponges collapse into a single master curve, clearly evident in both the panels of Figure 7. It should be pointed out that this master curve is obtained without any adjustable parameter. The values of ω_{BP} used to rescale both the frequency and the intensity of both INS and Raman data are plotted as a function of the molar ratio n in Figure 7c.

As already reported,[52−54,56,58] the existence of the scaling law summarized in Figure 7a,b provides evidence that the spectral shape of the BP, both in reduced VDOS and in the Raman intensity, is essentially the same for the three different investigated nanosponges. This finding supports the conclusion that the BP evolves according to the relative modifications of the elastic properties of the CDNS polymers, in good agreement with the trend observed for the Brillouin sound velocity measured on similar samples of nanosponges.[24]

In particular, all experimental data suggest a strong dependence on n of the stiffness of CDNS polymeric network, as summarized in the plots of Figure 7c. This finding confirms the conclusion that the molar ratio n is the variable affecting the elastic properties of nanosponges over the mesoscopic length scale.[24,27,29,30]

We remark that the same linear dependence on n of the frequency position ω_{BP} is observed in the reduced VDOS and Raman spectra (Figure 7c), supporting the reliability of the results previously discussed.

The close relationship found between the molar ratio n and the rigidity of the CDNS polymer matrix appears to be a result of considerable importance in view of the possible tunability of the macroscopic and functional properties of nanosponges. As a matter of fact, recent infrared spectroscopy measurements performed on hydrogels originated by swelling of β-CDPMA1n nanosponges[29,30] have demonstrated that the hydration of CDNS leads to the establishment of a hydrogen-bonds network involving the C═O functional groups of the polymers, whose connectivity pattern is strongly dependent on the parameter n. These findings are consistent with the conclusion that the elastic properties of nanosponges over the mesoscopic length scale play a key role in defining the macroscopic properties of CDNS hydrogel, like the water holding capacity and the rigidity of the gel network.

D. Frequency Dependence of the Raman Coupling Function. From the inspection of Figure 7c, as expected, the maxima of BP are found at higher energies in the inelastic light spectra with respect to the positions observed for the bump in the corresponding reduced VDOS. This is consistent with what was previously observed in other glass-forming systems,[33,59−61] and it is reflected in the spectral shape of the Raman coupling function $C(\omega)$, which has been estimated by the direct comparison between the experimental Raman and neutron scattering data, as described in the Theoretical Background section.

The Raman coupling function $C(\omega)$ measures the efficiency of the coupling between the incident photon and the vibrations of the system, and its frequency dependence plays a relevant role in clarifying the origin of the vibrational anomalies in disordered systems.[62]

In Figure 8, the frequency behavior of the Raman coupling function $C(\omega)$ calculated for the three investigated nanosponges is shown in the energy range 0−160 cm^{-1}. The profiles exhibit a complex spectral shape in the explored energy window: (i) for ω < 10 cm^{-1}, $C(\omega)$ decreases with increasing frequency; (ii) in the energy range of BP, that is, for 10 cm^{-1} < ω < 50 cm^{-1}, $C(\omega)$ values of all three types of CDNS show a

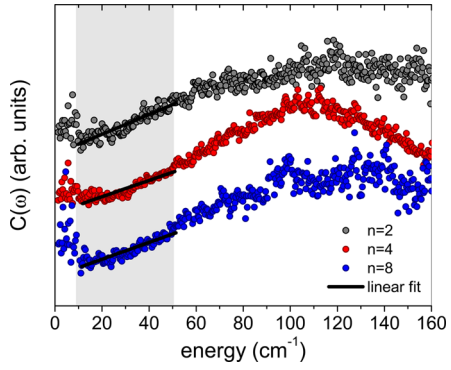

Figure 8. $C(\omega)$ calculated as described in the text for β-CDPMA1n nanosponges (n = 2, 4, 8) in the energy range 0−160 cm^{-1}. Different curves are vertically shifted for the sake of clarity. The gray region corresponds to the frequency range of the BP.

dx.doi.org/10.1021/jp410448y | J. Phys. Chem. B 2014, 118, 624−633

very similar frequency behavior that can be described by a linear dependence (see the gray region in Figure 8); and (iii) for $\omega > 50$ cm^{-1}, $C(\omega)$ tends to increase until it reaches a maximum centered at about 100−110 cm^{-1}.

This complex frequency behavior of $C(\omega)$ reflects the different kinds of excitations − localized vibrations, relaxations, high-frequency modes − contributing to the energy dependence of Raman coupling function in different frequency regimes.[48,59,60]

For $\omega < 10$ cm^{-1} the frequency dependence of $C(\omega)$ reflects the fact that the quasi-elastic scattering, which appears clearly in the Raman spectra of nanosponges (Figure 6b), tends to mask the true vibrational behavior of the Raman coupling function.

It is worth noting that in the energy range 10−40 cm^{-1}, $C(\omega)$ is found to show a linear frequency dependence for all samples of β-CDPMA1n nanosponges, thus explaining the shift to higher energies observed for the BP maximum in Raman scattering spectra with respect to neutron data.

To better analyze the spectral shape of $C(\omega)$, we compared the profiles of Figure 8 by rescaling the frequency axis in terms of $\nu = \omega/\omega_{BP}$, where ω_{BP} corresponds to the position of the maximum of BP observed in the reduced profiles of VDOS, $g(\omega)/\omega^2$ (Figure 6a).[62] Figure 9 shows the plot of Raman coupling function $C(\nu)$ for β-CDPMA1n nanosponges (n = 2, 4, 8) as function of the rescaled frequency ω/ω_{BP}. The curves were normalized near $\nu = \omega/\omega_{BP} = 1$.

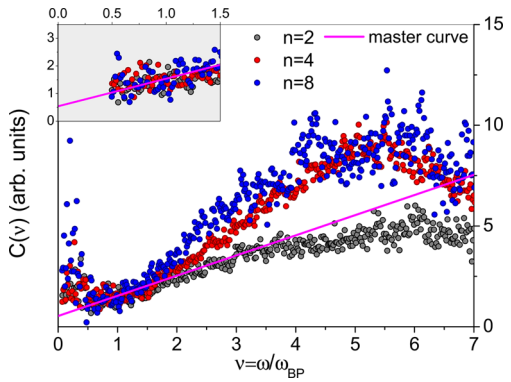

Figure 9. Frequency dependence of the Raman coupling function $C(\nu)$ as a function of the scaled frequency $\nu = \omega/\omega_{BP}$ for β-CDPMA1n nanosponges (n = 2, 4, 8) together with the master curve obtained for $0.5 < \nu < 1.5$. Inset: details of the low-frequency part of $C(\nu)$.

Interestingly, at frequency $0.5 < \omega/\omega_{BP} < 1.5$ (see inset of Figure 9), the $C(\nu)$ values corresponding to different samples of PMA-nanosponges tend to collapse into a single master curve, which is well described by the linear behavior:

$$C(\nu) \propto \omega/\omega_{BP} + 0.5 \quad (9)$$

This frequency dependence found at energies below $\sim 1.5\omega_{BP}$ is consistent with the universal behavior already observed on a large class of organic and inorganic glass-forming systems near the BP maximum.[62] The universal linear behavior described by eq 9 is common to disordered materials that are significantly different in type, structure, and fragility.[62]

Moreover, the occurrence of the same slope in the linear increase in $C(\nu)$ for PMA-nanosponges indicates that the BP evolution revealed in the Raman spectra of different kinds of nanosponges[24,27] indeed reflects the modifications in the VDOS of the system, independently of the coupling between the light and the polymer.

The different frequency dependence of $C(\nu)$ observed for $\omega/\omega_{BP} > 2$ for the three different types of nanosponges (Figure 9) is in agreement with the no-universality of the behavior of Raman coupling function already found in glasses.[60−62] This again reflects the different structures of CDNS polymers obtained by changing the parameter n during their synthesis and may strongly affect the high-frequency vibrations of the systems.

CONCLUSIONS

The vibrational dynamics of an innovative class of cross-linked polymers based on cyclodextrins was here investigated by combining Raman and INS experiments. By exploiting the complementarity of the two probes (light and neutron), in turn sensitive to different physical quantities, we explored the effect on the VDOS of the growing connectivity during the process of polycondensation of cyclodextrins leading to 3D cross-linked polymers.

In agreement with previous results, this study gave evidence that the motions of hydrogen atoms of CDNS are progressively hampered as the cross-linking degree of the covalent polymeric network increases.

The densities of vibrational states of nanosponges derived from INS spectra showed the presence of the characteristic anomalous excess of vibrational modes with respect to the harmonic Debye level already observed in the low-frequency Raman spectra of CDNS and referred to as the BP. The frequency and intensity of the BP were found to significantly change by increasing the cross-linking degree of the nanosponges network, as clearly supported by the existence of a scaling law for the BP evolution.

This finding suggested the interpretation that the spectral evolution of BP reflected the relative modifications of the elastic properties of the CDNS polymers, in turn, strictly dependent on the parameter n. Additionally, the linear trend of the Raman coupling function $C(\omega)$ versus frequency exhibited by the BP energy range, further confirmed that the BP evolution previously revealed in the Raman spectra of different kinds of nanosponges effectively reflected the modifications in the VDOS of the system independently of the coupling between light and the polymers.

The overall results contributed to complete the picture of the strict relationship between structural and functional properties of this new class of cross-linked polymers over the mesoscopic length scale. In perspective, the generality of the conclusions opens the possibility to exploit these methods as investigating tools for soft matter and amorphous materials.

AUTHOR INFORMATION

Corresponding Author

*E-mail: rossi@science.unitn.it. Tel: +39 0461 282940.

Notes

The authors declare no competing financial interest.

ACKNOWLEDGMENTS

We thank Dr. Marco Zanatta for useful discussions. Partial financial support from PRIN 2010 “Nanomed” is also acknowledged.

REFERENCES

(1) Hamley, I. W. *Introduction to Soft Matter: Synthetic and Biological Self-Assembling Materials*, revised ed.; Wiley & Sons: Hoboken, NJ, 2007.

(2) Rubinstein, M.; Colby, R. H. *Polymer Physics*; Oxford University Press, Inc.: New York, 2003.

(3) Sakurada, K.; McDonald, F. M.; Shimada, F. Regenerative Medicine and Stem Cell Based Drug Discovery. *Angew. Chem., Int. Ed.* **2008**, *47* (31), 5718−5738.

(4) Atala, A.; Lanza, R. P.; Thomson, J. A.; Nerem, R. M. *Principles of Regenerative Medicine*; Academic Press: Burlington, MA, 2008.

(5) Slaughter, B. V.; Khurshid, S. S.; Fisher, O. Z.; Khademhosseini, A.; Peppas, N. A. Hydrogels in Regenerative Medicine. *Adv. Mater.* **2009**, *21*, 3307−3329.

(6) Li, S.; Purdy, W. C. Cyclodextrins and Their Applications in Analytical Chemistry. *Chem. Rev.* **1992**, *92*, 1457−1470.

(7) Szejtli, J. Introduction and General Overview of Cyclodextrin Chemistry. *Chem. Rev.* **1998**, *98*, 1743−1753.

(8) Bender, M. L.; Komiyama, M. *Cyclodextrin Chemistry*; Springer-Verlag: New York, 1978.

(9) Trotta, F.; Tumiatti, W. Cross-Linked Polymers Based on Cyclodextrin for Removing Polluting Agents. Patent WO 03/085002, 2003.

(10) Trotta, F.; Tumiatti, W.; Cavalli, R.; Zerbinati, O.; Roggero, C. M.; Vallero, R. Ultrasound-Assisted Synthesis of Cyclodextrin-Based Nanosponges. Patent WO 06/002814, 2006.

(11) Trotta, F.; Tumiatti, W.; Cavalli, R.; Rogero, C.; Mognetti, B.; Berta, G. Cyclodextrin-Based Nanosponges as a Vehicle for Antitumoral Drugs. Patent WO 09/003656 A1, 2009.

(12) Subramanian, S.; Singireddy, A.; Krishnamoorthy, K.; Rajappan, M. Nanosponges: A Novel Class of Drug Delivery System − Review. *J. Pharm. Pharm. Sci.* **2012**, *15* (1), 103−111.

(13) Trotta, F.; Zanetti, M.; Cavalli, R. Cyclodextrin-Based Nanosponges as Drug Carriers. *Beilstein J. Org. Chem.* **2012**, *8*, 2091−2099.

(14) Lembo, D.; Swaminathan, S.; Donalisio, M.; Civra, A.; Pastero, L.; Aquilano, D.; Vavia, P.; Trotta, F.; Cavalli, R. Encapsulation of Acyclovir in New Carboxylated Cyclodextrin-Based Nanosponges Improves the Agent's Antiviral Efficacy. *Int. J. Pharm.* **2013**, *443*, 262−272.

(15) Minelli, R.; Cavalli, V.; Ellis, L.; Pettazzoni, P.; Trotta, F.; Ciamporcero, E.; Barrera, G.; Fantozzi, R.; Dianzani, C.; Pili, R. Nanosponge-Encapsulated Camptothecin Exerts Anti-Tumor Activity in Human Prostate Cancer Cells. *Eur. J. Pharm. Sci.* **2012**, *47*, 686−694.

(16) Torne, S. J.; Ansari, K. A.; Vavia, P. R.; Trotta, F.; Cavalli, R. Enhanced Oral Paclitaxel Bioavailability after Administration of Paclitaxel-Loaded Nanosponges. *Drug Delivery* **2010**, *17*, 419−425.

(17) Seglie, L.; Martina, K.; Devecchi, M.; Roggero, C.; Trotta, F.; Scaroiot, V. The Effect of 1-MCP in Cyclodextrin-Based Nanosponges to Improve the Vase Life of Dianthus Caryophyillus Cut Flowers Postharvest. *Biol. Technol.* **2011**, *59*, 200−205.

(18) Li, D.; Ma, M. Nanosponges: From Inclusion Chemistry to Water Purifying Technology. *Clean Prod. Processes* **2000**, *2*, 112−116.

(19) Swaminathan, S.; Pastero, L.; Serpe, L.; Trotta, F.; Vavia, P. R.; Aquilano, D.; Trotta, M.; Zara, G.; Cavalli, R. Cyclodextrin-Based Nanosponges Encapsulating Camptothecin: Physicochemical Characterization, Stability and Cytotoxicity. *Eur. J. Pharm. Biopharm.* **2010**, *74* (2), 193−201.

(20) Cavalli, R.; Akhter, A. K.; Bisazza, A.; Giustetto, P.; Trotta, F.; Vavia, P. Nanosponge Formulations as Oxygen Delivery Systems. *Int. J. Pharm.* **2010**, *402* (1−2), 254−257.

(21) Liang, W.; Yang, C.; Nishijima, M.; Fukuhara, G.; Mori, T.; Mele, A.; Castiglione, F.; Caldera, F.; Trotta, F.; Inoue, Y. Cyclodextrin Nanosponge-Sensitized Enantiodifferentiating Photoisomerization of Cyclooctene and 1,3-Cyclooctadiene. *Beilstein J. Org. Chem.* **2012**, *8*, 1305−1311.

(22) Liang, W.; Yang, C.; Zhou, D.; Haneoka, H.; Nishijima, M.; Fukuhara, G.; Mori, T.; Castiglione, F.; Mele, A.; Caldera, F. Y.; et al. Phase-Controlled Supramolecular Photochirogenesis in Cyclodextrin Nanosponges. *Chem. Commun.* **2013**, *49*, 3510−3512.

(23) Mele, A.; Castiglione, F.; Malpezzi, L.; Ganazzoli, F.; Raffaini, G.; Trotta, F.; Rossi, B.; Fontana, A. HR MAS NMR, Powder XRD and Raman Spectroscopy Study of Inclusion Phenomena in β CD Nanosponges. *J. Incl. Phenom. Macrocycl. Chem.* **2011**, *69* (3−4), 403−409.

(24) Rossi, B.; Caponi, S.; Castiglione, F.; Corezzi, S.; Fontana, A.; Giarola, M.; Mariotto, G.; Mele, A.; Petrillo, C.; Trotta, F.; et al. Networking Properties of Cross-linked Polymeric Systems Probed by Inelastic Light Scattering Experiments. *J. Phys. Chem. B* **2012**, *116* (17), 5323−5327.

(25) Castiglione, F.; Crupi, V.; Majolino, D.; Mele, A.; Rossi, B.; Trotta, F.; Venuti, V. Effect of Cross-linking Properties on the Vibrational Dynamics of Cyclodextrin-Based Polymers: An Experimental-Numerical Study. *J. Phys. Chem. B* **2012**, *116* (27), 7952−7958.

(26) Castiglione, F.; Crupi, V.; Majolino, D.; Mele, A.; Rossi, B.; Trotta, F.; Venuti, V. Inside New Materials: An Experimental-Numerical Vibrational Study of Cyclodextrins-Based Polymers. *J. Phys. Chem. B* **2012**, *116* (43), 13133−13140.

(27) Crupi, V.; Fontana, A.; Giarola, M.; Majolino, D.; Mariotto, G.; Mele, A.; Melone, L.; Punta, C.; Rossi, B.; Trotta, F.; et al. Connection Between the Vibrational Dynamics and the Cross-linking Properties in Cyclodextrins-based Polymers. *J. Raman Spectrosc.* **2013**, *44* (10), 1457−1462.

(28) Castiglione, F.; Crupi, V.; Majolino, D.; Mele, A.; Panzeri, W.; Rossi, B.; Trotta, F.; Venuti, V. Vibrational Dynamics and Hydrogen Bond Properties of β-CD Nanosponges: a FTIR-ATR, Raman and Solid-State NMR Spectroscopic Study. *J. Inclusion Phenom. Macrocyclic Chem.* **2013**, *75* (3), 247−254.

(29) Castiglione, F.; Crupi, F.; Majolino, D.; Mele, A.; Rossi, B.; Trotta, F.; Venuti, V. Vibrational Spectroscopy Investigation of Swelling Phenomena in Cyclodextrin Nanosponges. *J. Raman Spectrosc.* **2013**, *44* (10), 1463−1469.

(30) Crupi, V.; Majolino, D.; Mele, A.; Rossi, B.; Trotta, F.; Venuti, V. Modelling the Interplay between Covalent and Physical Interactions in Cyclodextrin-Based Hydrogel: Effect of Water Confinement. *Soft Matter* **2013**, *9*, 6457−6464.

(31) Raffaini, G.; Ganazzoli, F.; Mele, A.; Castiglione, F. A Molecular Dynamics Study of Cyclodextrin Nanosponge Models. *J. Inclusion Phenom. Macrocyclic Chem.* **2013**, *75* (3), 263−268.

(32) Hedoux, A.; Decroix, A.; Guinet, Y.; Paccou, L.; Derollez, P.; Descamps, M. Low- and High-Frequency Raman Investigations on Caffeine: Polymorphism, Disorder and Phase Transformation. *J. Phys. Chem. B* **2011**, *115*, 5746−5753.

(33) Crupi, V.; Fontana, A.; Giarola, M.; Guella, G.; Majolino, D.; Mancini, I.; Mariotto, G.; Paciaroni, A.; Rossi, B.; Venuti, V. Cyclodextrin-Complexation Effects on the Low-Frequency Vibrational Dynamics of Ibuprofen by Combined Inelastic Light e Neutron Scattering Measurements. *J. Phys Chem. B* **2013**, *117* (14), 3917−3926.

(34) Trotta, F.; Tumiatti, W.; Vallero, R. Nanospugne a Base di Ciclodestrine Funzionalizzate con Gruppi Carbossilici: Sintesi e Utilizzo nella Decontaminazione da Metalli Pesanti e da Composti Organici. Patent Number MI2004A000614

(35) Shuker, R.; Gammon, R. W. Raman-Scattering Selection-Rule Breaking and the Density of States in Amorphous Materials. *Phys. Rev. Lett.* **1970**, *25*, 222−225.

(36) Galenneer, F. L.; Sen, P. L. Theory for the First-Order Vibrational Spectra of Disordered Solids. *Phys. Rev. B* **1978**, *17*, 1928−1933.

(37) Carini, G.; D'Angelo, G.; Tripodo, G.; Fontana, A.; Leonardi, A.; Saunders, G. A.; Brodin, A. Excess of Low-Energy Excitations in Glasses. *Phys. Rev. B* **1995**, *52*, 9342−9353.

(38) Majolino, D.; Mallamace, F.; Migliardo, P.; Aliotta, F.; Micali, N.; Vasi, C. Spectral Evidence of Connected Structures in Liquid Water: Effective Raman Density of Vibrational States. *Phys. Rev. E* **1993**, *47*, 2669−2675.

(39) Bée, M. *Quasielastic Neutron Scattering: Principles and Applications in Solid-State Chemistry, Biology and Material Science*; Adam Hilger: Philadelphia, 1988.
(40) Lovesey, S. W. *Theory of Neutron Scattering from Condensed Matter*; Adair, R. K., Elliott, R. J., Krumhansl, J. A., Marshall, W., Wilkinson, D. H., Eds.; Clarendon Press: Ottawa, Ontario, 1986.
(41) Taraskin, S. N.; Elliott, S. R. Connection between the True Vibrational Density of States and that Derived from Inelastic Neutron Scattering. *Phys. Rev. B* **1997**, *55*, 117−123.
(42) Crupi, V.; Majolino, D.; Paciaroni, A.; Rossi, B.; Stancanelli, R.; Venuti, V.; Viliani, G. The Effect of Hydrogen Bond on the Vibrational Dynamics of Genistein Free and Complexed with β-cyclodextrins. *J. Raman Spectrosc.* **2010**, *41* (7), 764−770.
(43) Crupi, V.; Majolino, D.; Venuti, V.; Guella, G.; Mancini, I.; Rossi, B.; Verrocchio, P.; Viliani, G.; Stancanelli, R. Temperature Effect on the Vibrational Dynamics of Cyclodextrin Inclusion Complexes: Investigation by FTIR-ATR Spectroscopy and Numerical Simulation. *J. Phys. Chem. A* **2010**, *114* (25), 6811−6817.
(44) Chumakov, A. I.; Sergueev, I.; van Bürck, U.; Schirmacher, W.; Asthalter, T.; Rüffer, R.; Leupold, O.; Petry, W. Collective Nature of the Boson Peak and Universal Transboson Dynamics of Glasses. *Phys. Rev. Lett.* **2004**, *92*, 245508-1−245508-4.
(45) Paciaroni, A.; Orecchini, A.; Haertlein, M.; Moulin, M.; Conti Nibali, V.; De Francesco, A.; Petrillo, C.; Sacchetti, F. Vibrational Collective Dynamics of Dry Proteins in the Terahertz Region. *J. Phys. Chem. B* **2012**, *116* (12), 3861−3865.
(46) Maccarrone, S.; Magazù, S.; Migliardo, F.; Mondio, F. Small-angle Neutron Scattering and Inelastic Neutron Scattering Studies on β-cyclodextrins and Hydroxypropyl-β-cyclodextrins. *Physica B* **2004**, *350*, e615−e618.
(47) Kob, W.; Binder, K. *Glassy Materials and Disordered Solids: An Introduction*; World Scientific: London, 2011.
(48) Fontana, A.; Dell'Anna, R.; Montagna, M.; Rossi, F.; Viliani, G.; Ruocco, G.; Sampoli, M.; Buchenau, U.; Wischnewski, A. The Raman Coupling Function in Amorphous Silica and the Nature of the Long-Wavelength Excitations in Disordered Systems. *Europhys. Lett.* **1999**, *47* (1), 56−62.
(49) Fabiani, E.; Fontana, A.; Buchenau, U. Neutron Scattering Study of the Vibrations in Vitreous Silica and Germania. *J. Chem. Phys.* **2008**, *128* (24), 244507-1−244507-12.
(50) Rufflé, B.; Ayrinhac, S.; Courtens, E.; Vacher, R.; Foret, M.; Wischnewski, A.; Buchenau, U. Scaling the Temperature-Dependent Boson Peak of Vitreous Silica with the High-Frequency Bulk Modulus Derived from Brillouin Scattering Data. *Phys. Rev. Lett.* **2010**, *104* (6), 067402-1−067402-4.
(51) Benassi, P.; Fontana, A.; Frizzera, W.; Montagna, M.; Mazzacurati, V.; Signorelli, G. Disorder-Induced Light Scattering in Solids: The Origin of the Boson Peak in Glasses. *Philos. Mag.* **1995**, *71* (4), 761−769.
(52) Monaco, A.; Chumakov, A. I.; Yue, Y. Z.; Monaco, G.; Comez, L.; Fioretto, D.; Crichton, W. A.; Rüffer, R. Density of Vibrational States of a Hyperquenched Glass. *Phys. Rev. Lett.* **2006**, *96*, 205502-1−205502-4.
(53) Orsingher, L.; Fontana, A.; Gilioli, E.; Carini, G.; Carini, G.; Tripodo, G.; Unruh, T.; Buchenau, U. Vibrational Dynamics of Permanently Densified GeO2 Glasses: Densification-Induced Changes in the Boson Peak. *J. Chem. Phys.* **2010**, *132* (12), 124508-1−124508-5.
(54) Zanatta, M.; Baldi, G.; Caponi, S.; Fontana, A.; Gilioli, E.; Krish, M.; Masciovecchio, C.; Monaco, G.; Orsingher, L.; Rossi, F.; et al. Elastic Properties of Permanently Densified Silica: A Raman, Brillouin Light and X-ray Scattering Study. *Phys. Rev. B* **2010**, *81*, 212201-1−212201-4.
(55) Pilla, O.; Angelani, L.; Fontana, A.; Gonçalves, J. R.; Ruocco, G. Structural and Dynamical Consequences of Density Variation in Vitreous Silica. *J. Phys.: Condens. Matter* **2003**, *15*, S995−S1005.
(56) Hong, L.; Begen, B.; Kisliuk, A.; Alba-Simionesco, C.; Novikov, V. N.; Sokolov, A. P. Pressure and Density Dependence of the Boson Peak in Polymers. *Phys. Rev. B* **2008**, *78*, 134201-1−134201-11.
(57) Deschamps, T.; Martinet, C.; de Ligny, D.; Bruneel, J. L.; Champagnon, B. Correlation between Boson Peak and Anomalous Elastic Behavior in GeO_2 Glass: An in Situ Raman Scattering Study under High-Pressure. *J. Chem. Phys.* **2011**, *134*, 234503-1−234503-4.
(58) Caponi, S.; Corezzi, S.; Fioretto, D.; Fontana, A.; Monaco, G.; Rossi, F. Raman-Scattering Measurements of the Vibrational Density of States of a Reactive Mixture During Polymerization: Effect on the Boson Peak. *Phys. Rev. Lett.* **2009**, *102*, 027402-1−027402-4.
(59) Fontana, A.; Rossi, F.; Viliani, G.; Ruocco, G.; Dal Maschio, R. The Raman Coupling Function in Disordered Solids: a Light and Neutron Scattering Study on Glasses of Different Fragility. *J. Phys.: Condens. Matter* **2007**, *19*, 1−6.
(60) Fontana, A.; Rossi, F.; Fabiani, E. The Raman Coupling Function in v-GeO2 and v-SiO2: A New Light and Neutron Scattering Study. *J. Non-Cryst. Solids* **2006**, *352*, 4601−4605.
(61) Ivanda, M.; Kiefer, W.; Mariotto, G. Raman Light-to-Vibration Coupling Coefficient of v-SiO2 in Spectral Interval Range up to 600 cm^{-1}. *Solid State Commun.* **2001**, *117*, 423−428.
(62) Surovtsev, N. V.; Sokolov, A. P. Frequency Behviour of Raman Coupling Coefficient in Glasses. *Phys. Rev. B* **2002**, *66*, 054205-1−054205-6.